Detachment of agglutinin-bonded red blood cells

I. Forces to rupture molecular-point attachments

E. Evans,*‡ D. Berk,* and A. Leung*
*Departments of Pathology and ‡Physics, University of British Columbia, Vancouver, British Columbia, V6T 1W5, Canada

ABSTRACT A simple micromechanical method has been developed to measure the rupture strength of a molecular-point attachment (focal bond) between two macroscopically smooth membrane capsules. In the procedure, one capsule is prepared with a low density coverage of adhesion molecules, formed as a stiff sphere, and held at fixed position by a micropipette. The second capsule without adhesion molecules is pressurized into a spherical shape with low suction by another pipette. This capsule is maneuvered to initiate point contact at the pole opposite the stiff capsule which leads to formation of a few (or even one) molecular attachments. Then, the deformable capsule is slowly withdrawn by displacement of the pipette. Analysis shows that the end-to-end extension of the capsule provides a direct measure of the force at the point contact and, therefore, the rupture strength when detachment occurs. The range for point forces accessible to this technique depends on the elastic moduli of the membrane, membrane tension, and the size of the capsule. For biological and synthetic vesicle membranes, the range of force lies between 10^{-7}–10^{-5} dyn (10^{-12}–10^{-10} N) which is 100-fold less than presently measurable by Atomic Force Microscopy! Here, the approach was used to study the forces required to rupture microscopic attachments between red blood cells formed by a monoclonal antibody to red cell membrane glycophorin, anti-A serum, and a lectin from the snail-helix pomatia. Failure of the attachments appeared to be a stochastic function of the magnitude and duration of the detachment force. We have correlated the statistical behavior observed for rupture with a random process model for failure of small numbers of molecular attachments. The surprising outcome of the measurements and analysis was that the forces deduced for short-time failure of 1–2 molecular attachments were nearly the same for all of the agglutinin, i.e., 1–2 × 10^{-6} dyn. Hence, microfluorometric tests were carried out to determine if labeled agglutinins and/or labeled surface molecules were transferred between surfaces after separation of large areas of adhesive contact. The results showed that the attachments failed because receptors were extracted from the membrane.

INTRODUCTION

Agglutination and other adhesive reactions are controlled by the immune system through formation of small numbers of molecular bridges between membrane surfaces (1, 1*a*). Most of these contacts are initiated in situations where external forces act to disrupt the contact (e.g., in the blood circulation); consequently, the strength of molecular attachments is very important for the viability of cell aggregates in vivo. Estimates of forces required to break single agglutinin crossbridges have been deduced from a variety of theoretical and experimental considerations (2, 3). However, previous experimental approaches have usually involved indirect or complicated procedures that could not be adequately analyzed to give precise values for force per microscopic attachment. A notable exception was the controlled disruption of point contacts between two rigid spheres in a fluid shear field (4, 5). Specifically, two-cell aggregates of red blood cells (chemically fixed by glutaraldehyde as rigid spheres) were separated to obtain estimates of the forces required to rupture microscopic attachments produced with antisera (5). The rupture forces were spread over a broad range from 10^{-6}–10^{-5} dyn; estimates of the discrete force to break a single molecular crossbridge were deduced from the lowest values measured, 1–2 × 10^{-6} dyn. Unfortunately, this elegant approach does not allow cells to be assembled and detached in an easily controlled manner. As such, the duration of force application cannot be extended so that time-dependent features of failure can be examined.

We describe here a direct method to measure the strength (rupture force) for microscopic focal bonds between membrane surfaces. For reasons to be outlined later, the range of "point" forces f accessible to this technique is limited to $10^{-7} < f < 10^{-5}$ dyn ($10^{-12} < f < 10^{-10}$ N) for common biological and surfactant membranes. By comparison, these forces are ~100-fold lower than the present level of sensitivity of sophisticated techniques like the Atomic Force Microscope (6). The simple method is based on a "spring-like transducer" for force. The force "transducer" is the extension of a pressurized membrane capsule held under constant membrane tension. In the procedure to form point attachments, care is taken to minimize the

Address correspondence and reprint requests to Dr. Evans.

0006-3495/91/04/838/11 $2.00

initial contact area and the adhesive surface is prepared with a low density of sites for adhesion. With this approach, we have studied the strengths of point contacts produced by several agglutinins. The agglutinins chosen for these tests included a monoclonal antibody to red cell membrane glycophorin A, the snail-helix pomatia-lectin (which binds to A blood-group antigens), and anti-A serum. Rupture forces were found to depend on duration of the detachment process; however, forces for rapid (1–5 s) detachment were closely grouped in value. The results indicated that the microscopic mechanism of failure was a similar stochastic process for each type of agglutinin. For rapid detachment, the probable value of rupture force appeared to represent either a single- or double- molecular attachment.

In any measurement of force required to separate an adhesive contact (single point or macroscopic region), the actual locus of molecular failure is difficult to determine. It is like "pulling carrots out a garden: the gardener's grip on the carrot may be broken without removing the carrot; the green-leafy top may break-off in the gardener's hand; or the whole carrot may be extracted from the soil." Similarly, rupture of a single molecular cross-bridge may occur at the binding site, or the complex may break internally at another location, or the receptor may be extracted from the membrane bilayer. Because covalent linkages within molecules are very strong, it is likely (but not certain) that molecules will remain intact. Consequently, it would seem that either the ligand-receptor bond or extraction from the membrane will be the site of rupture. To indicate the locus of contact "fracture," we describe results from microfluorometric tests designed to determine if either labeled agglutinins and/or labeled surface molecules were transferred between surfaces after separation of large adhesion areas.

MICROMECHANICAL TEST PROCEDURE

Even if the origin of failure is unknown, it is important to determine the strength characteristics of single molecular contacts. For this purpose, a simple procedure was developed and used to study agglutinin bonds. Conceptually, two membrane capsules in the form of nearly perfect spheres are maneuvered by small micropipettes to form a "point" contact at their poles. In advance, one of the capsules is prepared with a low density of surface sites for adhesion. After assembly, the capsules are separated to test the strength of the contact. In the studies presented here, the membrane capsules were human red blood cells as shown in Fig. 1. (Other smooth membrane capsules can also be used, e.g., phospholipid bilayers reconstituted with receptor molecules). Each red blood cell was selected from a separate chamber on the microscope stage. The capsule on the right was taken from a cell suspension previously incubated with the agglutinin, monoclonal antibody or lectin, at low concentration (just sufficient to cause occasional adhesion). This cell had either been chemically cross-linked in the form of a rigid sphere or was a normal cell pressurized by very large suction to create a stiff sphere outside the pipette. The micropipette with the stiff cell was held at a fixed position. The capsule on the left was a normal cell chosen from a suspension in phosphate buffered saline, 0.1 M, plus a small amount of albumin to prevent crenation and adhesion to glass, but no agglutinin. This cell was slightly preswollen by osmotic hydration so it could be aspirated into a spherical form by low pipette suction without a membrane crease or fold inside the tube. The low-pressure cell was maneuvered to just touch the stiff cell at the pole with a small region of contact (Fig. 1 *a*), then withdrawn to test for adhesion. Sometimes a microscopic adhesive bond was formed but other times not. (No adhesion occurred without agglutinin.) Pushing the cells together produced large flat regions of contact which usually led to large detachment forces due to multiple adhesion sites. (Formation and separation of large adhesive contacts are described in a companion paper [7] for the same agglutinins.) Finally, at constant suction pressure, the pipette on the left was steadily retracted until the cell detached from the polar contact. Because the cell membrane tension was low, the cell contour was elongated slightly by the action of the small axial force at the polar contact (Fig. 1 *b*). At detachment, the total end-to-end extension of the deformable cell was accurately measured by electronic video-image analysis of the pipette displacement.

MATERIALS AND METHODS

Agglutinins

Three different agglutinins were studied with this technique. The first was a monoclonal antibody (molecular weight of ~150,000 daltons) to the integral membrane protein glycophorin A (provided as a gracious gift by Dr. M. Narla, University of California, San Francisco). The antibody (R10 MAb) binds to a region that is ~45 Å distal from the bilayer (between residues 25 and 40; references 8 and 9). This antibody is an IgG with two binding sites, the minimum needed to form a cross-bridge. The second agglutinin molecule was the lectin (HPA) from the snail-helix pomatia. This lectin (molecular weight of ~79,000 daltons) consists of six subunits, each with a binding site for an *N*-acetylgalactosamine residues associated with the blood-type A antigens (10). We also investigated the forces to rupture attachments produced by antiserum to blood-type A antigens. Anti-A serum is a heterogeneous mixture of immunoglobulins, primarily IgM's that are pentagonal arrangements of IgG (1, 1*a*). Cells to be used as the stiff test surface were incubated with each agglutinin for over 1 h in a

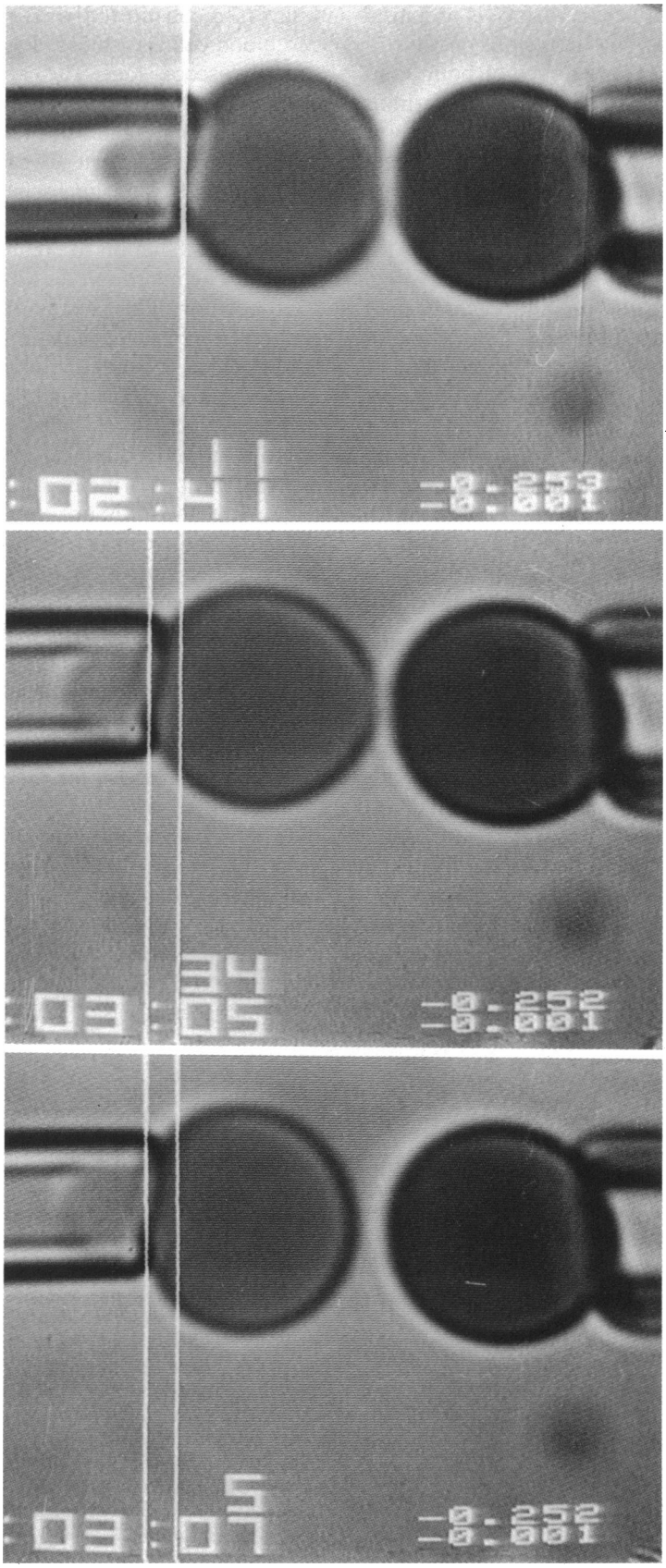
02:41
-0.253
-0.001
03:05
-0.252
-0.001
03:07
-0.252
-0.001

slightly hypotonic (160 mOsm) phosphate-buffered saline solution (pH 7.4) with 1 g% human serum albumin. The cell suspension was very dilute ($\sim 5 \times 10^5$ cells/ml) and the concentration of agglutinin was in the range 10^{-9}–10^{-8} M for the MAb and 10^{-10}–10^{-9} M for the lectin. Based on our studies of binding with the lectin and MAb's, the surface density of agglutinin molecules was estimated to be well below 10% of the saturation value (i.e., <40,000 molecules/cell or $< 3 \times 10^{10}$ molecules/cm^2).

Micromanipulation

For micromanipulation of cells, small micromanipulators were mounted on the stage of a Leitz inverted microscope. Glass micropipettes with internal diameters of 2–3 μm were attached and connected to micrometer-driven water manometers for pressure adjustment. The pipette pressure was displayed on a video monitor and recorded with the microscope image. A crucial feature was the facility to transfer cells between different chambers on the microscope stage. Adjacent fluid-filled chambers were arranged on the stage, each separated by a narrow air gap. In one chamber, a small micropipette was used to select and insert a cell into a large pipette (internal diameter 10–20 μm). The microscope stage was then translated to move the concentric pipettes through the air gap to a separate environment without exposing the cell. In this way, test cells were selected from a chamber that contained buffer solution with antibody or lectin and transferred to an adjacent chamber that contained normal red blood cells in buffer without agglutinin molecules. In the second chamber, the osmolarity of the buffer solution was adjusted to 160–200 mOsm to preswell the flaccid cells as shown in Fig. 1. The solution contained human serum albumin (1 g/100 ml) to prevent adhesion of normal cell membrane to the glass micropipette.

Rigid red cell substrates

For some tests, rigid-spherical test surfaces were created by chemical fixation of swollen red blood cells with use of an established procedure (5). A drop of human type A blood was collected and washed three times with 0.1 M sodium phosphate buffer (240 mOsm, pH 7.6, with 1.2 mM $MgCl_2$). Four microliters of washed packed cells were added to 500 μl of buffer containing 3.3 μl of lysolecithin (1 mg/ml ethanol solution). The suspension of swollen red blood cells was then treated with the cross-linking agent DSP (3,3-dithiobis propionic acid *N*-hydroxy-succinimide ester); 3.13 μl of DSP dissolved in DMSO (dimethylsulfoxane) (160 mg/ml) was added to the suspension to yield a final concentration of 1 mg/ml DSP. The cells were incubated for ~1 h at room temperature and then washed several times in buffer. To ensure that no cross-linking activity remained, the cells were incubated in 0.2 M glycine for another hour and washed several more times. Fixation was verified by suspension of the cells in distilled water where they retained their hemoglobin. These spheres could be stored in distilled water at 4°C for periods of months. Although the surfaces appeared macroscopically smooth and spherical, scanning electron micrographs have revealed some surface roughness on the nanometer scale (5). The average diameter of these spheres was less than 6×10^{-4} cm so swelling and fixation resulted in some loss of cell surface area.

Microfluorometry

A microfluorometry system was used to study transfer of fluorescently labeled molecules between adherent cell pairs after separation. The system, similar to that described in reference 13, utilizes a Coherent Optics (CA) 4-W argon-ion laser as the illumination source. The laser beam is first modulated and attenuated, then enters the microscope to epi-illuminate (through the objective) the cell surface. The image of the beam on the object surface can either be focussed to a spot, diffuse, or other patterns as determined by the beam conditioning optics. Fluorescence from labeled molecules on the surface (or within the cell cytoplasm) passes through the dichroic mirror to produce an image at the microchannel plate-intensified video camera (Lenzar Corp, FL) or to be sampled by an optical fiber connected to a photomultiplier tube. The video intensity is quantitated either by electronic digitization (Matrox Video Processor, Quebec, Canada) of the video image or by a photon discriminator-counter system and fed directly to the memory of a microprocessor. A microcomputer controls the illumination level and fluorescence recording sequences appropriate to the desired experimental format.

To test for transfer of agglutinin and/or receptors between adherent cell membranes after separation, the following microfluorometric experiments were performed: in all tests, large areas of adhesive contact were created between two red cells by mechanical impingement (7). One red cell was always selected from a suspension of cells chemically fixed as rigid spheres; the other cell was taken from a suspension of normal cells. Before the tests, the rigid spherical cells were prebound with agglutinin (either R10 MAb or HPA) at concentrations sufficient to produce high levels of surface binding (~ 5–10×10^5/cell). This procedure was chosen to facilitate maximum formation of agglutinin cross-bridges and to avoid aggregation of receptors on the surface before cell–cell contact. Two different protocols were used to discriminate between agglutinin transfer, and receptor transfer, after the adherent cells were separated: (*a*) in the first approach, fluorescently labeled MAb or lectin was bound to the rigid cell surface. After cell pairs were separated, the normal cell was examined for fluorescence which would show that agglutinin molecules were transferred. (Note: the practical limit to detection with the microfluorometric system was ~1/50 of the initial surface density of fluorescence.) (*b*) In the second approach, normal red cells were labeled with fluorescein (following established procedures) which appears to label mainly the integral proteins of the red cell membrane (14). Thus, it was likely the band 3 and glycophorin were the principal sources for fluorescence from the labeled cells. (Cell pairs were agglutinated with unlabeled agglutinin.) After cell pairs were separated, the rigid spherical cell was examined for fluorescence which would show that receptor molecules were transferred.

MECHANICAL ANALYSIS

Deformation of the cell contour from the initial spherical form provided a direct measure of the point force at the polar contact. This is analogous to the displacement

FIGURE 1 Videomicrograph sequence of assembly and detachment of red blood cells bonded by molecular-point attachments. The cell on the right was either pressurized by high suction to form a stiff sphere or was a cell chemically fixed as a sphere. The cell on the left was pressurized at low suction. (*a*) Cells were assembled to make contact at the poles. (*b*) The cell on the left was displaced to test for adhesion and to apply force on the attachment. The force at polar contact extended the cell. (*c*) The cells shown after displacement; the vertical cursors demonstrate the measurement of displacement.

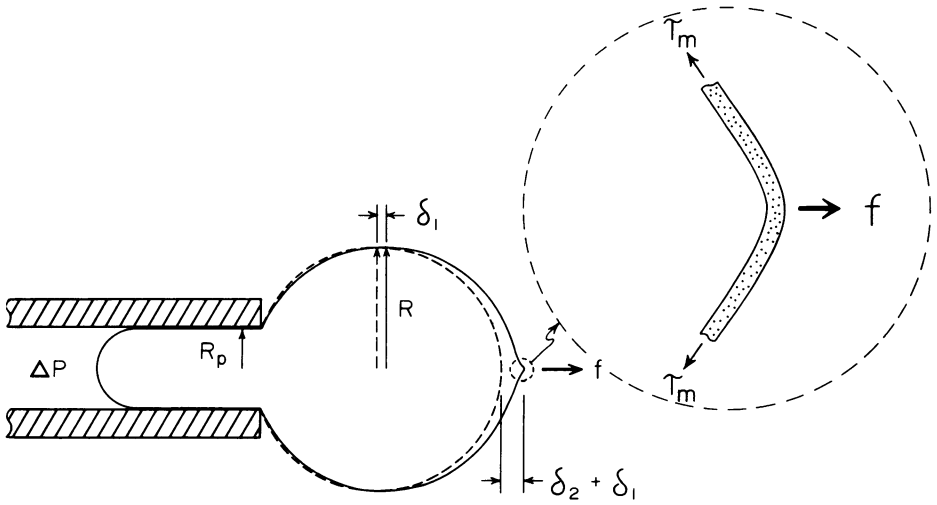

FIGURE 2 Schematic of a membrane capsule sectioned into regions for analysis of deformation. The first region is well approximated by a surface of constant mean curvature. Most of the second region is also well approximated by the same constant mean curvature contour *except* for the region around the point load (illustrated in the cut-out). In the region local to the point of force, membrane bending rigidity (aided by shear rigidity) stiffens the contour to "blunt" the deformation as shown.

of a taut elastic wire in proportion to a transverse load. However, the mechanical analysis is slightly more complicated for the membrane capsule. Over most of the capsule away from the polar contact, the spherical membrane contour is deformed into a nonspherical surface with constant total curvature (sum of the two principal curvatures = constant) as predicted by membrane mechanics (11).[1] Simple analysis of the capsule membrane envelope predicts that the point load will extrude an arbitrary-length membrane cylinder (a "tether" or hollow filament) from the pole (12). This is due to idealization of the membrane as a thin surface with no bending rigidity. The "tether" diameter ($2r_t$) is simply determined by the balance of axial force (i.e., $2\pi r_t \tau_m \simeq f$, where τ_m is the membrane tension and f is the force). Thus, the small bending rigidity (plus shear rigidity in some cases) of the membrane must be included in the analysis. When bending rigidity is considered, the membrane shape near the microscopic point load is stiffened to form a smooth-closed contour (illustrated in Fig. 2). To perform the analysis, the cell is divided into two regions: (*a*) the region from the pipette entrance to the equatorial cross-section at radius R; and (*b*) the region from the equator to the polar contact point. Before detachment, the axial length of the first section is given by

$$\ell_o = R \cdot \sqrt{1 - (R_p/R)^2}$$

and the initial length of the second section is defined by R_o. As detachment proceeds, the point force extends both cell regions as shown in Fig. 2. Away from the region local to the polar contact (where bending and shear rigidities are important), the contour is well approximated by constant total curvature. Thus, for small displacements, extension of the first region is given by

$$\delta_1/R = K_1 \tilde{f}\,(1 + \tilde{f}),$$

where

$$K_1 = \ln\,[(1 + \ell_o/R) \cdot R/R_p]$$

$$\tilde{f} = f/(2\pi R \tau_m).$$

In the second region, bending rigidity (aided by shear rigidity) stabilizes the membrane contour near the polar contact as shown in the cut-out in Fig. 2. Extension of the second region is much larger and, because of more complex mechanics, must be evaluated by numerical computation. The computational algorithm is based on smooth continuation of the solution for the contour over the bending (and shear) dominated region near the

[1]The "liquid" membrane approximation can be used to model most of the cell membrane (i.e., constant isotropic tension) because the tension was sufficient to exceed the surface shear rigidity as evidenced by the spherical shape in Fig. 1 *a*. However, the small shear rigidity stiffens the membrane region near the point load as described in the Appendix.

point load into the large-scale contour defined by constant total curvature (outlined in the Appendix). The result takes the form,

$$\delta_2/R = K_2\tilde{f} + K_3\tilde{f}^2,$$

where K_2 and K_3 are functions of $\tilde{B} = B/\tau_m R_o^2$ and $\tilde{\mu} = \mu/\tau_m$. B is the elastic bending modulus of the membrane (typically 10^{-12} erg for red cell and lipid bilayer membrane); μ is the elastic shear modulus of the membrane (zero for lipid bilayers with liquid acyl chains and $\sim 10^{-2}$ dyn/cm for red cell membranes). Finally, a small correction is required to account for the change in equatorial radius as the cell is extended, given by,

$$\delta_c/R = (R_o - R)/R + \sqrt{(R_o/R)^2 - (R_p/R)^2} - \sqrt{1 - (R_p/R)^2},$$

where R_o is the initial radius of the sphere and R is the equatorial radius of the extended cell. Thus, the total end-to-end extension of the capsule is represented by the sum of fractional displacements as given by,

$$\delta/R_o = (\delta_1 + \delta_2 - \delta_c)/R.$$

This sum provides the "transducer" relation for displacement of the capsule (from its initial position defined by the spherical shape) in proportion to the point force (Fig. 3). As shown in Fig. 3, end-to-end extension of the capsule is not greatly affected by the magnitude of the bending modulus as long as the bending stiffness is sufficient to prevent formation of a cylindrical tether. With red blood cells, two criteria are important: the displacement δ must be $<0.5 \times R_o$, the radius of the capsule, and the tension τ_m must satisfy the inequalities, $\tau_m > f^2/(2\pi)^2 B$ and $\tau_m > \mu$. The small shear rigidity of the red cell membrane allows the capsule to be extended to greater lengths ($\delta/R_o \sim 0.5$) before a tether is produced. (The initial extension of the capsule [$\delta/R_o < 0.2$] depends only on the bending rigidity and is essentially independent of the membrane shear modulus.) When these conditions are met, then force and displacement depend only on the membrane tension and the size of the capsule as shown in Fig. 3. Membrane tension is controlled by the pipette suction pressure ΔP [e.g., $\tau_m \simeq \Delta P R_p/2(1 - R_p/R_o)$]; therefore, the sensitivity to force can be altered through control of the pipette suction. For red cell and lipid bilayer capsules, the practical limits for point forces are bounded by 2×10^{-7} dyn at the low end (because optical diffraction and detection restrict observations to $\sim 0.2 \times 10^{-4}$ cm) and by $\sim 6 \times 10^{-6}$ dyn at the high end (because membrane tethers form at larger forces). This range could easily be extended to include much larger forces if the membranes are chemically cross-linked to increase stiffness.

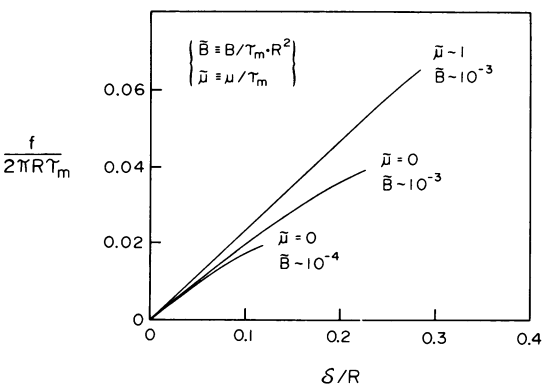

FIGURE 3 Based on the analysis of extensions for the sections illustrated in Fig. 2, the total displacement δ of the membrane capsule is related to the force f applied at the polar contact. Force is scaled by membrane tension $\tau_m \times$ cell radius R_0 and displacement by cell radius to establish universal "transducer" relations for force vs. displacement. These depend on characteristic stiffness ratios, $\tilde{B} = B/\tau_m R_0^2$ and $\tilde{\mu} = \mu/\tau_m$, for membrane bending and shear rigidities vis a vis membrane tension. (The tension level is established by pipette suction pressure according to, $\tau_m \simeq \Delta P R_p/2[1 - R_p/R_0]$.)

RESULTS

Rupture forces

Because the stiff cell surface was bound with a low density of agglutinin, adhesive contacts were only observed in ~50% of the attempts to point-agglutinate cells. When large initial contact areas were forced by mechanical impingement and held for long periods before separation, the frequency of attachments increased significantly and often led to macroscopic-size adhesive contacts. Thus, efforts were made to "standardize" the initial contact by using the same pipette suction pressure, holding contact for the same period of times before separation, and limiting contact area to a similar small size (just at the level of optical detection). Identification of cell pairs as "nonadherent" was equivalent to detachment forces below the detection level of 2×10^{-2} dyn. Cell pairs that appeared adherent could easily be discriminated because the force was at least a few times larger than the detection threshold. For rapid detachment within 1–5 s, detachment forces grouped in the same range for all of the agglutinins as cumulated in Table 1 (forces in excess of 6–7 $\times 10^{-6}$ dyn led to formation of long cylindrical tethers and thus could not be measured). For these tests, the rate of pipette displacement was approximately constant (about 0.4×10^{-4} cm/s), equivalent to a constant rate of force increase (~ 1–2×10^{-6} dyn/s). Because displacements were small, the rate of detachment did not produce

TABLE 1 **Forces for rapid (< 5 s) detachment of different agglutinins**

Agglutinin	Minimum force	Maximum force	Average force	Standard deviation	*n*
	10^{-6} *dyn*	10^{-6} *dyn*	10^{-6} *dyn*	10^{-6} *dyn*	
anti-A Serum	0.7	3.8	2.0	0.7	50
HPA	0.6	4.5	2.0	0.8	44
R10 MAb	0.5	4.5	2.1	1.0	115

significant viscous dissipation in either the cell membrane or the adjacent fluids. For each type of agglutinin, measurements of rupture forces were cumulated into the histograms shown in Fig. 4. No significant difference was observed between distributions of detachment forces measured in tests where the stiff cells were taken from suspensions of osmotically swollen normal red cells or chemically fixed red cell spheres as shown in Fig. 4. The forces clustered around low values of 1–2 × 10^{-6} dyn.

As shown in Fig. 4, force measurements for the agglutinins grouped in the same range of values; but there was no clear demonstration of discrete rupture forces in the results. Measurement uncertainties were expected to create a spread of only 2 × 10^{-7} dyn; thus, the continuous distribution must have been due to other stochastic effects. This is not surprising when the assembly/detachment processes are considered more carefully as follows: it is reasonable to assume that assembly led to formation of only a small number of discrete attachments because of the low surface density of agglutinin, small contact area, and infrequent bonding after contact. For a single bond held at fixed force, the probability of survival most likely attenuates with the duration of the load. Further, the survival time is expected to decrease as the force is increased. Hence, even though a few (even one) molecular attachments are involved, failure becomes a continuous stochastic function of the magnitude and duration of the applied force. To examine these features, we carried out another series of detachment tests to determine time-dependent properties of failure. Hence, constant forces were applied by initial displacement of the cell (in <1 s) to a fixed position; the force level was set in the range of 0.2–3.0 × 10^{-6} dyn. Then, the time interval required for failure of the attachment was recorded. The range of forces was chosen because most adherent cell pairs were observed to separate within 1–5 s with forces below 2 × 10^{-6} dyn. As expected (especially at low forces), detachment was not immediate as shown in Fig. 5; the intervals varied from 1 s to more than a minute. More than 80% of the cell pairs were separated by forces between 0.6–1.2 × 10^{-6} dyn if given sufficient time.

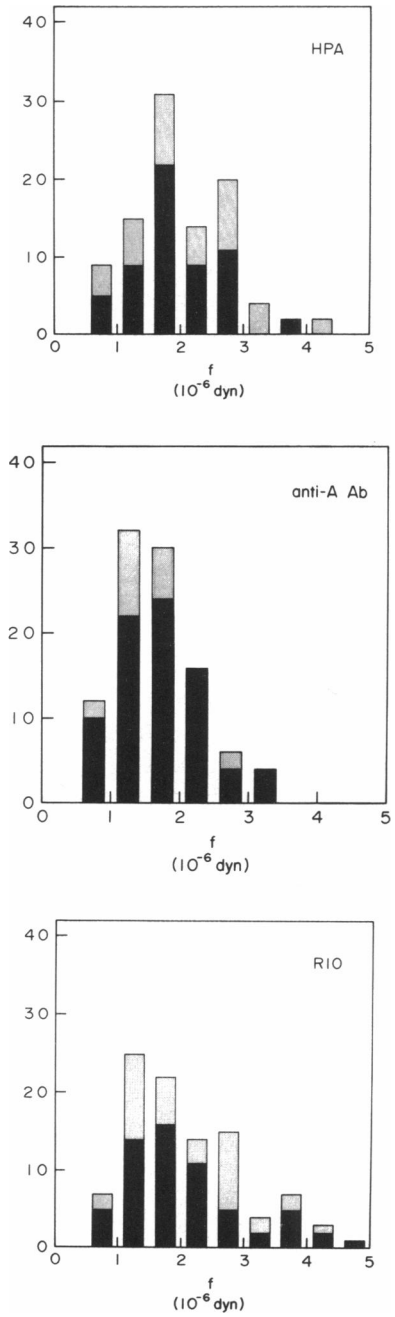

FIGURE 4 Forces measured for rapid detachment (<1–5 s) of red cells bonded at microscopic points by three different agglutinins. The cells were withdrawn at a steady rate of 0.4 × 10^{-4} cm/s. The histograms cumulate rupture forces for cells attached by each agglutinin as follows: (*a*) the lectin HPA and (*b*) anti-A serum which bind to blood type A antigens; (*c*) R10 monoclonal antibody to red cell membrane glycophorin. The solid portions represent data for cells detached from chemically fixed RBC's; the cross-hatched portions are data for cells detached from normal RBC's pressurized into stiff spheres.

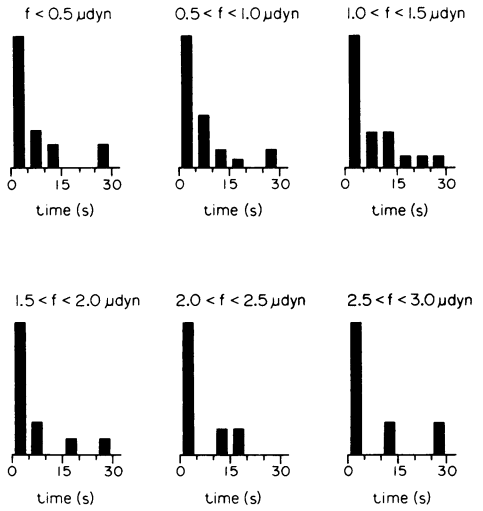

FIGURE 5 Histograms of the fraction of microscopic-point attachments that ruptured in 5-s time intervals for cell–cell contacts held at fixed force levels. Cells were agglutinated by R10 monoclonal antibody to red cell membrane glycophorin. Each histogram includes more than 20 tests; however, the vertical scales have been normalized to give the same numbers for failure by rapid detachment (0–5 s) in each force range so as to show the time dependence.

Agglutinin and/or receptor transfer

As stated in the introduction, the origin of failure for molecular attachments is most likely either the agglutinin-receptor bond or the extraction of receptors from the membrane. Thus, we performed fluorescence "transfer" studies as described in the Methods section. When cell pairs were separated which had been agglutinated by fluorescent R10 MAb, there was no detectable fluorescence "footprint" left on the deformable cell. The fluorescent antibody remained bound to the chemically fixed test cell. However, when cell pairs were separated where the deformable cell membrane had been fluorescenated, an obvious fluorescence "footprint" was left on the rigid spherical cell. These observations strongly indicated that, when bonded by the antibody, receptors were physically extracted from the normal red cell membrane (but not the chemically fixed cell). On the other hand for cell pairs agglutinated with the lectin HPA, it was found that a fluorescence "footprint" was left on the unlabeled surface after separation in both cases. However, when the label was the fluorescentated proteins of the flaccid cell, the transfer of label was weak in comparison to the situation where the lectin (bound to the fixed cell surface) was labeled. This was not surprising since it is thought that the lectin binds to glycolipids. Hence, transfer of label from the fluorescentated to flaccid cell was likely due to proteins associated with the glycolipid receptors or there may have been a few binding sites for the lectin on minor glycoproteins.

DISCUSSION

Analysis of rupture as a random process

The absence of clearly identifiable discrete forces necessitates a more detailed consideration of bond failure. The results show that the probability of survival is never entirely one or zero; also, reduction in the likelihood of survival varies over a significant range of force. For surfaces bonded by noncovalent attachments, it has been predicted that no force is needed to separate the surfaces; eventually a bond will spontaneously dissociate (2). Similarly, it has been shown that dissociation rates and average survival times will vary strongly with the mechanical force on the attachment (15). Similar features are clearly evident in our results (Fig. 5). In addition, it is unlikely that the entire range of detachment forces can be attributed to a single attachment. The distribution of detachment forces (Figs. 4 and 5) probably reflects the failure of a few bonds; but each attachment may not have experienced the same force history. Distribution of the detachment force amongst attachment sites is difficult to predict because of microscopic irregularities, "roughness," over the bonded region as discussed in a companion paper (7).

To illustrate the stochastic nature of microscopic "fracture" and to demonstrate how a few discrete failures lead to a continuous distribution of force, we introduce a random process concept for rupture of microscopic contacts. (This approach is well established in the study of reliability of electronic components [16]. An outline of the derivation is presented in Appendix II.) Fig. A1 in the appendix shows probability densities for failure as a function of number of attachments. It is apparent that the most likely time for failure at a given load shifts progressively to larger values with more bonds but the spread in times becomes larger as well. Finally, the expectation time for "fracture" of a microscopic adhesion area will depend on the number of attachments formed on initial assembly which varies with each assembly attempt. If formation of discrete bonds on initial contact is Poisson distributed, the probability densities for failure of different sets of n bonds (Fig. A1) must be superposed to create a single probability density for the average $\langle n \rangle$. It is clear that a simple stochastic theory for failure can predict the dynamic features of the detachment process. Unfortunately, insufficient data were obtained to provide precise correlation with different mechanisms of failure (e.g., as

a function of the exponent "a"). However, because the times for rupture were strongly skewed toward short durations for all values of rupture force, it is likely that the most probable number of molecular rupture events was close to one. Also, the moderate frequency of attachments ($\sim 50\%$) after initial assembly is consistent with a single rupture site (as is readily derived from the properties of a Poisson distribution). Hence, we conclude that the rupture force at a histogram peak (Fig. 4) represents the level of force required to rapidly disrupt a single molecular attachment. The deduction is reasonable based on the small size of the initial contact ($< 10^{-8}$ cm^2), the average distance between adhesive sites ($\sim 10^{-5}$ cm based on surface density of agglutinin), and the infrequent occurrence of attachments after assembly attempts. Even though geometric calculations predict that several attachments could be formed in the small area at initial contact, microscopic surface "roughness" can reduce this number significantly.

Locus of failure

Surprisingly, molecular-point attachments formed by the agglutinins (lectin, R10 monoclonal antibody, and anti-A immunoglobulin) appeared to require comparable levels of force for short-time rupture ($1\text{–}2 \times 10^{-6}$ dyn). Receptors for these agglutinins were both integral membrane proteins (glycophorin for the MAb, maybe other proteins for some antibodies in the anti-A serum) and membrane glycolipids (for the lectin and anti-A serum). This seems to be paradoxical: i.e., different agglutinins, different receptors, but the same rupture force per site. However, the fluorescence transfer studies provide a rationalization for the unexpected behavior. The results indicated that receptors were extracted from the membrane at separation and that the agglutinin remained attached to the receptor. Thus, the deduction is that the rupture force represented a common process of molecular extraction from a hydrophobic bilayer core. The values measured here for average rupture force are consistent with estimates of the force required to extract a receptor from a liquid bilayer (i.e., $\sim 2.6 \times 10^{-6}$ dyn, reference 2). If we accept the conclusion that receptors were extracted from the membrane, it would also explain why only a single rupture event appeared to occur even though more than one agglutinin bond may have been involved: i.e., the receptors would be drawn together by the detachment force to form a microscopic aggregate which would then be extracted from the membrane surface. As such, it is expected that the detachment force would only increase with the square root of the number of receptors in the aggregate (based on the hydrophobic perimeter). For this scenario, the aggregate would have included no more than 4–5 receptors to be consistent with the force measurements.

APPENDIX 1

Finite-difference approach to obtain membrane shape

As noted in the text, the membrane region from the pipette entrance to the equator of the cell body was treated as a fully pressurized capsule with a geometry given by constant mean curvature $\bar{c}_o$ (sum of principal curvatures = constant). In this region, the membrane stresses reduce to an isotropic tension $\bar{\tau}$ (analogous to a liquid membrane surface) which is related to the pipette suction pressure (ΔP), pipette, and cell body radii (R_p, R), and the mean curvature by,

$$2\bar{\tau} = \Delta P \cdot R_p/(2 - R_p/R - R \cdot \bar{c}_o/2). \quad \text{(A1)}$$

The mean curvature is determined by the point force (scaled by tension and cell radius), i.e.

$$\bar{c}_o = 2(1 - \bar{f})/R$$

$$\bar{f} \equiv f/(2\pi R \cdot \bar{\tau}). \quad \text{(A2)}$$

On the other side of the equator, the geometry was derived from the full equations of mechanical equilibrium for the membrane, including bending and shear rigidities. The solutions were matched at the equator such that the membrane orientation (given by the angle θ between the local normal and axis of symmetry), curvatures, and meridional tension were continuous to first order. Calculation of the shape was accomplished by means of a finite-difference algorithm for the complete equations. The unsupported region of the capsule was

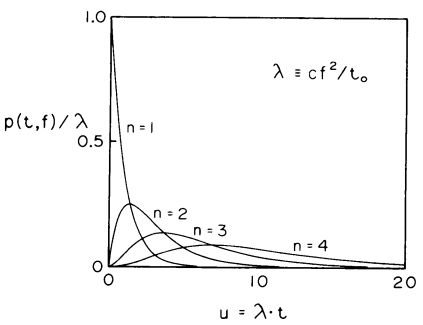

FIGURE A1 Density of probability that a contact with n attachments will "fracture" within a small interval about time t when held at constant force f. The exponent "a" scales the dependence of microscopic frequency of failure on the force and here was chosen as $a = 2$ to represent an energy-dependent frequency of failure. Probability densities are plotted for total failure from one to four molecular attachments. It is assumed that failure of the attachments is a sequence of random events. The probability density is scaled by the microscopic frequency of rupture for a single attachment ($\lambda = c \cdot f^a/t_0$).

approximated as a series of conical sections, each with a mean radius r and surface orientation angle θ at a meridional position s. The surface area and volume of this region of the cell are simply the sums of the areas and volumes for each of the conical sections. These sections were mapped back to an undeformed cell shape to determine the reference coordinates s_0 and r_0, the initial meridional position and the initial radial distance from the axis of symmetry. This "map" established the local extension (shear deformation) of each membrane section which specifies the shear resultant τ_s. The shear resultant is defined by the difference between principal membrane tensions and is determined with the local membrane extension ratio λ_m as given by (11),

$$\tau_s = \frac{\mu}{2}(\lambda_m^2 - \lambda_m^{-2}) \text{ and } \lambda_m = r_0/r. \tag{A3}$$

Because the effects of shear rigidity were only significant near the point load, the undeformed reference shape was taken as a sphere of radius R. This choice facilitated the continuity of membrane shape and stress at the equator. For this reference geometry, the deformation map that specifies the extension ratio (at constant surface density) is given by matching equivalent areas,

$$R(1 - \cos\theta_0) = \int_0^r \frac{r' \cdot dr'}{\cos\theta}$$

$$\lambda_m = R \cdot \sin\theta_0/r.$$

The balance of forces along the axis of symmetry and the differential balance of membrane stresses tangent to the surface were used to specify the local mechanical equilibrium for the membrane (11), i.e.,

$$\epsilon_1 = u \cdot \tau_m - B(1 - u^2) \cdot \frac{\partial \bar{c}}{\partial r} - \frac{f}{2\pi r} - \frac{r \cdot p_c}{2}$$

$$\epsilon_2 = \frac{\partial \tau_m}{\partial r} + B\left(\bar{c} - \frac{u}{r}\right)\frac{\partial \bar{c}}{\partial r} + \frac{u}{r}(\lambda_m^2 - \lambda_m^{-2}). \tag{A4}$$

These balances define second order, nonlinear, coupled differential equations in the dependent variable u which represents the membrane orientation through $u = \sin\theta$ and yields a simple expression for mean curvature, $\bar{c} = [\partial(ru)/\partial r]/r$. Eqs. A4 specifies the residual functions ϵ_1 and ϵ_2 that were linearized and used in a finite difference algorithm to obtain the solution for the membrane shape and the tension at any point. For small changes in r and u, the perturbation in the functions ϵ are given by first order linear expansions:

$$\Delta\epsilon_1 = \frac{\partial \epsilon_1}{\partial r} \cdot \Delta r + \frac{\partial \epsilon_1}{\partial u} \cdot \Delta u + \frac{\partial \epsilon_1}{\partial\left(\frac{\partial \bar{c}}{\partial r}\right)} \cdot \Delta\left(\frac{\partial \bar{c}}{\partial r}\right) + \frac{\partial \epsilon_1}{\partial \tau_m} \cdot \Delta\tau_m$$

$$\Delta\epsilon_2 = \frac{\partial \epsilon_2}{\partial r} \cdot \Delta r + \frac{\partial \epsilon_2}{\partial u} \cdot \Delta u + \frac{\partial \epsilon_2}{\partial \bar{c}} \cdot \Delta\bar{c} + \frac{\partial \epsilon_2}{\partial\left(\frac{\partial \bar{c}}{\partial r}\right)} \cdot \Delta\left(\frac{\partial \bar{c}}{\partial r}\right)$$

$$+ \frac{\partial \epsilon_2}{\partial\left(\frac{\partial \tau_m}{\partial r}\right)} \cdot \Delta\left(\frac{\partial \tau_m}{\partial r}\right) + \frac{\partial \epsilon_2}{\partial \lambda_m} \cdot \Delta\lambda_m$$

$$\Delta\lambda_m = -\lambda_m \cdot \Delta r/r. \tag{A5}$$

The deviations Δr and Δu must be kept small so that the linear expansion remains valid. To do this, either small increments in point load were applied in series or viscous dissipation was added to the shear elasticity. With dissipation, a time step is chosen to create a quasi-elastic response with magnitude proportional to the deviation from equilibrium. Thus, the viscous resistance to membrane deformation regulates the relaxation to the equilibrium shape. Even when the starting shape is far from true equilibrium, the transient force creates a quasi-equilibrium geometry. The relaxation process occurs over discrete time steps Δt; the step size is chosen to ensure that Δr and Δu are small. The quasi-elastic tension component is introduced into Eq. A3 with the definition,

$$\tau_s \simeq \frac{\mu}{2}(\lambda_m^2 - \lambda_m^{-2}) + 2t_v \cdot \Delta\lambda_m/\Delta t, \tag{A6}$$

where t_v is the characteristic viscoelastic time constant. For computational purposes, t_v is chosen arbitrarily so that $\Delta t/t_v$ at each step is small enough to ensure convergence. This is verified by diminishing the interval until the solution does not change.

The membrane is divided into n segments; at each segment ($i = 1$ to n), the changes in r and u must satisfy:

$$\epsilon + \Delta\epsilon \simeq 0, \tag{A7}$$

where u and r are related by the geometrical relation

$$\frac{dr}{ds_0} = \lambda_m \cdot (1 - u^2)^{1/2}. \tag{A8}$$

Thus the perturbations in u and r are governed by

$$\Delta\left(\frac{dr}{ds_0}\right) = -\lambda_m\left[\frac{(1 - u^2)^{1/2}}{r}\Delta r + u(1 - u^2)^{-1/2}\Delta u\right]. \tag{A9}$$

The finite-difference approximations yield a linear system of equations. The solution must satisfy the following boundary conditions: first, since the angle θ approaches zero at the pole faster than the radius (because of the bending stiffness), the simple approach was to choose a small value for the radius r^* where $u = 0$. Provided that r^* was sufficiently small (< 0.1 μm), the solution did not depend on the value. (A more rigorous approach was also tested. This involved an analytic expansion of the solution around $r = 0$ but no differences were found so the simple method was implemented. Specification of r^* was equivalent to inserting a small rigid platelet in the membrane at the point load.) Next at $r = R$ (the equator), both the angle ($\theta = \pi/2$ or $u = 1$) and the mean curvature were required to be continuous (equal to the values from the liquid membrane solution) to first order as given by

$$\Delta u = 0$$

$$0 = (\bar{\tau} \cdot \bar{c} - P_c) + \bar{\tau} \cdot \Delta\bar{c} + (\bar{c} - 2/R) \cdot \Delta\tau_s.$$

APPENDIX 2

Random process model for rupture of microscopic attachments

The probability for survival of a single molecular attachment will depend on applied force and duration (time) of the load. The likelihood that an attachment will fail in a subsequent short time interval is proportional to an instantaneous frequency of failure $\lambda(t, f)$ given that the attachment has survived to time t. Here, we assume that failure is a random event characterized by a "lifetime" t_c, i.e., $\lambda \sim 1/t_c$.

Rate reaction theories predict that the "lifetime" should decrease as force is applied to the attachment (2); thus, the "lifetime," or inverse of the frequency of microscopic failure, is modeled by a phenomenological relation as

$$t_c = t_0 \cdot \mathrm{EXP}\,[-c \cdot f^a]$$
$$\lambda = \mathrm{EXP}\,[c \cdot f^a]/t_0 \simeq (c/t_0) f^a,$$

where t_0 and c are phenomenological-constitutive-constants. We replace the exponential dependence on force with a characteristic exponent "a". (A value for $a = 2$ would indicate an energy-dependent frequency of failure.) Thus, the probability $S(t, f)$ for survival up to time t with the force held at f decreases as a negative exponential function of the integral of the microscopic rate of failure over time, i.e.

$$s(t,f) = \mathrm{EXP}\,[-\int_0^t \lambda \cdot dt'] = \mathrm{EXP}\,[-(c/t_0) f^a \cdot t].$$

The likelihood of failure in the next short interval of time is the product of the survival probability x fractional rate of failure given as,

$$p(t,f) = \lambda \cdot S(t,f).$$

The probability density function for failure of a single attachment is given by

$$p(t,f) = u \cdot e^{-u}/t,$$

where $u \equiv cf^a t$. The probability that n attachments fail is easily derived from the assumption that the time intervals between individual failures are described by a random process. However, as failure progresses, the subtle feature is that the load f will be distributed amongst a diminishing number of attachments. Thus, the instantaneous failure rate will depend on the number of survivors at time t according to

$$\lambda_k = (k \cdot c/t_0)\,(f/k)^a, \qquad \hat{t}_{k-1} < t < \hat{t}_k,$$

where t_k is the failure time for one out of k attachments. The probability density for failure of all n attachments follows from the distribution of total time for detachment given by the sum of the random intervals t_k. The result is a superposition of exponential functions,

$$p(t,f) = \lambda_1 \left\{ \sum_{k=1}^{n} \left[\frac{e^{-u/k^{a-1}}}{k^{a-1} \prod_{\ell \neq k}^{n} (1 - (\ell/k)^{a-1})} \right] \right\}$$

given here for $a > 1$. Fig. A1 shows the probability densities for failure as a function of number of attachments where the exponent "a" was chosen equal to 2 to represent energy-dependent failure. If the frequency of failure scales linearly with force ($a = 1$), then the probability density for failure is given by the "gamma" function distribution (16),

$$p(t,f) = \lambda u^{n-1} e^{-u}/(n-1)!$$

A force-based frequency of failure would characterize viscous-like yield of attachments. In the case of extraction of membrane receptors from a lipid bilayer core, it is likely that the process would exhibit this type of behavior ($a \cong 1$) with perhaps a small threshold.

This work was supported by the U.S. National Institutes of Health grant HL45099.

Received for publication 13 February 1990 and in final form 6 December 1990.

REFERENCES

1. Mollison, P. L. 1983. Blood Transfusion in Clinical Medicine. 7th ed. Blackwell Scientific Publications, Oxford. 988 pp.
1a. Sell, S. 1987. Immunology, Immunopathology, and Immunity. 4th ed. Elsevier, New York. 852 pp.
2. Bell, G. I. 1978. Models for the specific adhesion of cells to cells. *Science (Wash. DC).* 200:618–627.
3. Bongrand, P. 1988. Physical Basis of Cell–Cell Adhesion. CRC Press, Boca Raton, FL. 267 pp.
4. Tha, S. P., and H. L. Goldsmith. 1986. Interaction forces between red cells agglutinated by antibody. I. Theoretical. *Biophys. J.* 50:1109–1116.
5. Tha, S. P., J. Shuster, and H. L. Goldsmith. 1986. Interaction forces between red cells agglutinated by antibody. II. Measurement of hydrodynamic force of breakup. *Biophys. J.* 50:1117–1126.
6. Binnig, G., C. F. Quate, and C. H. Gerber. 1986. Atomic force microscope. *Phys. Rev. Lett.* 56:930–933.
7. Evans, E., D. Berk, A. Leung, and M. Narla. 1990. Detachment of agglutinin-bonded red blood cells: II. Mechanical energies to separate large contact areas. *Biophys. J.* 59:849–860.
8. Ridgwell, K., M. J. A. Tanner, and D. J. Anstee. 1983. The Wr^b antigen, a receptor for plasmodium falciparum malaria, is located on a helical region of the major membrane sialoglycoprotein of human red blood cells. *Biochem. J.* 209:273–276.
9. Anstee, D. J., and P. A. W. Edwards. 1982. Monoclonal antibodies to human erythrocytes. *Eur. J. Immunol.* 12:228–232.
10. Hammarstrom, S., and E. A. Kabat. 1971. Studies on specificity and binding properties of the blood group A reactive hemagglutin from Helix pomatia. *Biochemistry.* 10:1684–1692.
11. Evans, E., and R. Skalak. 1980. Mechanics and Thermodynamics of Biomembranes. CRC Press, Inc., Boca Raton, FL. 254 pp.
12. Hochmuth, R. M., and E. Evans. 1982. Extensional flow of erythrocyte membrane from cell body to elastic tether. I. Analysis. *Biophys. J.* 39:71–81.
13. McGregor, G. N., H.-G. Kapitza, and K. Jacobson. 1984. Laser-based fluorescence microscopy of living cells. *Laser Focus/Electro-Optics.* 20:85–93.
14. Golan, D. E., and W. Veatch. 1980. Lateral mobility of band 3 in the human erythrocyte membrane by fluorescence photobleaching recovery: evidence for control by cytoskeletal interactions. *Proc. Natl. Acad. Sci. USA.* 77:2537–2541.
15. Dembo, M., D. C. Torney, K. Saxman, and D. Hammer. 1988. The reaction-limited kinetics of membrane-to-surface adhesion and detachment. *Proc. R. Soc. Lond. B.* 234:55–83.
16. Beckmann, P. 1967. Probability in Communication Engineering. Harcourt, Brace and World, Inc., New York. 511 pp.